The Astronomical Journal, 162:214 (6pp), 2021 November https://doi.org/10.3847/1538-3881/ac2739

Keck/OSIRIS Paβ High-contrast Imaging and Updated Constraints on PDS 70b

Taichi Uyama[1,2,3], Chen Xie[4], Yuhiko Aoyama[5,6], Charles A. Beichman[1,2], Jun Hashimoto[7,8], Ruobing Dong[9], Yasuhiro Hasegawa[10], Masahiro Ikoma[3], Dimitri Mawet[10,11], Michael W. McElwain[12], Jean-Baptiste Ruffio[11], Kevin R. Wagner[13,14,16], Jason J. Wang[11,17], and Yifan Zhou[15,18]

[1] Infrared Processing and Analysis Center, California Institute of Technology, 1200 E. California Boulevard, Pasadena, CA 91125, USA; tuyama@ipac.caltech.edu
[2] NASA Exoplanet Science Institute, Pasadena, CA 91125, USA
[3] National Astronomical Observatory of Japan, 2-21-1 Osawa, Mitaka, Tokyo 181-8588, Japan
[4] Aix Marseille Univ, CNRS, CNES, LAM, Marseille, France
[5] Institute for Advanced Study, Tsinghua University, Beijing 100084, People's Republic of China
[6] Department of Astronomy, Tsinghua University, Beijing 100084, People's Republic of China
[7] Astrobiology Center, 2-21-1 Osawa, Mitaka, Tokyo 181-8588, Japan
[8] Subaru Telescope, National Astronomical Observatory of Japan, Mitaka, Tokyo 181-8588, Japan
[9] Department of Physics & Astronomy, University of Victoria, Victoria, BC V8P 1A1, Canada
[10] Jet Propulsion Laboratory, California Institute of Technology, 4800 Oak Grove Drive, Pasadena, CA 91109, USA
[11] Department of Astronomy, California Institute of Technology, 1200 E. California Boulevard, Pasadena, CA 91125, USA
[12] Exoplanets and Stellar Astrophysics Laboratory, Code 667, Goddard Space Flight Center, Greenbelt, MD 20771, USA
[13] Steward Observatory, University of Arizona, Tucson, AZ 85721, USA
[14] NASA NExSS Alien Earths Team, USA
[15] Department of Astronomy/McDonald Observatory, The University of Texas, 2515 Speedway, Stop C1400 Austin, TX 78712, USA
Received 2021 July 12; revised 2021 August 13; accepted 2021 September 14; published 2021 October 26

Abstract

We present a high-contrast imaging search for Paβ line emission from protoplanets in the PDS 70 system with Keck/OSIRIS integral field spectroscopy. We applied the high-resolution spectral differential imaging technique to the OSIRIS *J*-band data but did not detect the Paβ line at the level predicted using the parameters of Hashimoto et al. (2020). This lack of Paβ emission suggests the MUSE-based study may have overestimated the line width of Hα. We compared our Paβ detection limits with the previous Hα flux and Hβ limits and estimated A_V to be ~0.9 and 2.0 for PDS 70 b and c, respectively. In particular, PDS 70 b's A_V is much smaller than implied by high-contrast near-infrared studies, which suggests the infrared-continuum photosphere and the hydrogen-emitting regions exist at different heights above the forming planet.

Unified Astronomy Thesaurus concepts: Exoplanet astronomy (486); Planet formation (1241)

1. Introduction

A variety of theoretical and observational studies have investigated planet formation, yet the mechanisms are still poorly understood. High-contrast imaging at infrared (IR) wavelengths can detect the thermal emission of young exoplanets directly and thus provide key insights to distinguish between various planet formation mechanisms. Characterization of the physical and atmospheric parameters of protoplanets at specific ages helps in assessing the initial conditions of their formation (e.g., Bonnefoy et al. 2014). Furthermore, addressing such problems as reconciling the evolutionary cooling models (hot/warm/cold start; Spiegel & Burrows 2012) with the relevant physical processes (e.g., core accretion and disk instability; Pollack et al. 1996; Boss 1997) are essential to improving our understanding of planet formation. One of the ways to probing planet formation is to observe hydrogen emission originating in active mass accretion onto protoplanets (Aoyama et al. 2018).

PDS 70 is one of the most intriguing young systems with high-contrast imaging, revealing two protoplanets located within a large cavity of the protoplanetary disk (PDS 70bc; Keppler et al. 2018; Haffert et al. 2019) and follow-up observations confirming active mass accretion onto them (e.g., Haffert et al. 2019). Previous studies have explored some of the hydrogen-emission lines in the PDS 70 system; Hα (656.28 nm), Hβ (486.14 nm), Brα (4.050 μm), and Brγ (2.166 μm). Hα emission has been reported by MagAO (Wagner et al. 2018), VLT/MUSE (Haffert et al. 2019), and HST (Zhou et al. 2021). The measured Hα flux shows temporal variability on a 1–2 yr timescale for reasons that are still controversial: either systematic instrumental calibration errors and/or an intrinsic time variability. The MUSE data include Hβ line but yielded only a null detection (Hashimoto et al. 2020) with 3σ upper limits of 2.3 and 1.6×10^{-16} erg s^{-1} cm^{-2} for PDS 70 b and c, respectively. Christiaens et al. (2019) reported the *K*-band spectrum of PDS 70 b taken by VLT/SINFONI ($R \sim 100$) and Wang et al. (2021) presented the *K*-band spectra of PDS 70 bc taken by VLT/GRAVITY (MEDIUM resolution), but they did not detect significant Brγ emission. Wang et al. (2021) set 3σ upper limits of Brγ to 5.1 and 4.0×10^{-17} erg s^{-1} cm^{-2} for PDS 70 b and c, respectively, which are limited by the *K*-band continua of PDS 70 bc. Stolker et al. (2020) reported the detection of PDS 70 bc with VLT/NACO NB4.05 filter (Brα filter; $\lambda_{\rm cen} = 4.05$ μm, $\Delta\lambda = 0.02$ μm). However, they suggested that PDS 70 b's spectrum is best fit by an atmospheric model without Brα and did not argue in favor of a line detection. In addition to the hydrogen-emission lines, Zhou et al. (2021) reported ultraviolet (UV) emission from PDS 70 b with HST/WFC F336W filter and suggested that the hydrogen continuum emission dominates the UV flux. Aoyama et al. (2020) incorporated all these lines into a discussion of the emission mechanisms but were unable to determine fully the physical and accretion parameters of PDS 70 bc.

[16] NASA Hubble Fellowship Program—Sagan Fellow.
[17] 51 Pegasi b Fellow.
[18] Harlan J. Smith McDonald Observatory Fellow.

Table 1
OSIRIS Observations using the Jn3 Filter with the Plate Scale of 20 mas

Target	$t_{\rm DIT} \times n_{\rm DIT}$[a]	On-source Time (s)
PDS 70	40 × 120	4800[(b)]
HD 143956	20 × 1	20
HD 144609	2 × 1	2

Note.
[a] $t_{\rm DIT}$ is the exposure time per image frame in the unit of seconds and $n_{\rm DIT}$ is the number of image frames.[b] The last eight frames were excluded in the analysis due to the inferior observing conditions, resulting in a practical total integration time of 3840 s.

Here we report on a search for the previously unobserved line of Paβ (1.282 μm) around PDS 70 which is one of the brightest emission lines relative to Hα. We used Keck/OSIRIS mid-resolution integral field spectroscopy (IFS; $R \sim 4000$) to further investigate the accretion mechanisms of PDS 70 bc. The observations and preliminary result of the postprocessing were originally reported in Uyama et al. (2021). In this paper we present the updated results with a detailed analysis of the data following Xie et al. (2020; see Sections 2 and 3). Section 4 investigates constraints on the accreting parameters of PDS 70 bc by incorporating the OSIRIS results with the previous studies.

2. Data

2.1. Observations

We observed PDS 70 with Keck/OSIRIS in the Jn3-band on 2020 May 31 UT (PI: Charles Beichman) to search for a Paβ emission line (1.282 μm) from accretion onto the protoplanets. We used the OSIRIS IFS spatial sampling of 0.″02 spaxel^{-1} that covers a field of view of 0.″96 × 1.″28, where each spatial location has a spectrum from 1.275 μm to 1.339 μm (Jn3) with resolving power of ∼4000. The observations achieved a total exposure time of 4800 s (120 s single exposure×40 frames) under good seeing conditions (0.″4–0.″6). The typical full width half maximum (FWHM) of the PDS 70's point-spread function (PSF) measured a diffraction-limited ∼60–70 mas, but the quality of the last sequence of the observations was poor because of high airmass (>2.2) and relatively bad seeing (∼0.″7). Hence we excluded the last eight frames from this analysis. By taking the ratio of the flux within a 3-by-3-spaxel aperture and within the entire field of view (FoV), we estimated the Strehl ratio to be 9.88% at Paβ. Due to the relatively small FoV (0.″96 × 1.″28), we may overestimate the Strehl ratio. The low Strehl ratio (typically <20%) can lead to flux loss and we took into account this effect in the data analysis. We also obtained unsaturated images of HD 143956 (spectral type: B9; Houk & Smith-Moore 1988) and HD 144609 (spectral type: K0; Houk & Smith-Moore 1988) for telluric correction and photometric reference, respectively. The details of the OSIRIS observations can be found in Table 5.

2.2. Data Reduction

We used the OSIRIS Data Reduction Pipeline (reduction type: astronomical reduction pipeline; Lyke et al. 2017; Lockhart et al. 2019) with the corresponding rectification matrices[19] to extract the data cube and calibrated for dark subtraction, cosmic-ray removal, telluric correction, and wavelength solution. To search for faint companions with single emission lines, we need to first subtract the stellar light accurately. The preliminary data reduction presented in Uyama et al. (2021) applied the PCA-based SDI reduction that was originally used for the MUSE data (Hashimoto et al. 2020). However, this reduction technique left some instrumental residuals due to sensitivity differences between the OSIRIS spaxels. We therefore applied an advanced high-resolution spectral differential imaging (HRSDI) technique to remove the stellar emission (see Haffert et al. 2019 and Xie et al. 2020 for the details). HRSDI is suitable for retrieving sharp emission lines while removing the stellar halo. However, before we applied the HRSDI to the final combined data set, some residual bad pixels were removed from each exposure that passed through the OSIRIS Data Reduction Pipeline. To remove the bad pixels, we first applied HRSDI on each exposure, aiming for reducing the influence of stellar emission in the next step. Next, we applied a sigma clipping algorithm on the dithered exposures to make a bad pixel mask for each exposure. Then all the exposures were centered on the flux peak and mean combined after the removal of bad pixels.

The process of HRSDI consists of two steps, removing the stellar emission and removing the uncalibrated instrumental effects. The stellar emission was subtracted from all normalized spaxels with the normalized reference spectrum that was obtained after the continuum normalization (Haffert et al. 2019). The uncalibrated instrumental residuals were removed using a principal component analysis (PCA) subtraction technique (Amara & Quanz 2012; Soummer et al. 2012). For example, the instrumental residual in Uyama et al. (2021) can be removed with the first few PCA components. The number of PCA components to subtract was determined by maximizing the signal-to-noise ratio of injected fake planets at the location of PDS 70 b (see also Section 2.3).

2.3. Fake Planet Injection

To estimate the instrumental throughput, we performed the fake planet injection described in Xie et al. (2020). The instrumental throughput includes the flux loss due to the low Strehl ratio (see Section 2.1) and that made by the PSF subtraction. Unless we specifically mentioned, both effects were corrected throughout the paper. The fake planet was created based on a planet spectrum and a stellar PSF. We used a single Gaussian line as the planet spectrum because our observations did not utilize angular differential imaging and thus did not achieve sufficient contrast to detect the continua of PDS 70 bc. We adopted the line-of-sight redshift of 25 km s^{-1} (Haffert et al. 2019) and a FWHM of 70 km s^{-1} or 0.3 nm. The injected Gaussian line can be covered by two spectral channels. We measured the flux using the aperture photometry in spectral channels of 1281.75 nm and 1281.90 nm with a square aperture of 3-by-3 spaxels (60 × 60 mas). The noise was estimated at the same spatial location in the spectral direction after HRSDI, using 150 spectral channels (bandwidth: 22.5 nm) around Paβ. After obtaining a 5 σ detection, we estimated the flux loss caused by the PSF subtraction by comparing the injected and recovered flux. The flux losses caused by the PSF subtraction are 28% and 14% at the location of PDS 70 b and c, respectively.

[19] http://tkserver.keck.hawaii.edu/osiris/

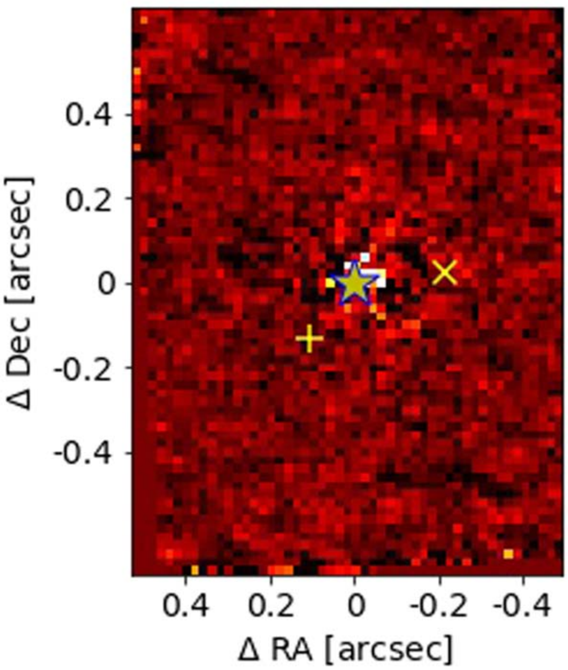

Figure 1. The HRSDI-reduced Keck/OSIRIS data at wavelengths of 1281.75 and 1281.9 nm (combined image). The locations of PDS 70, PDS 70 b, and c are indicated by the star, plus, and cross symbols, respectively.

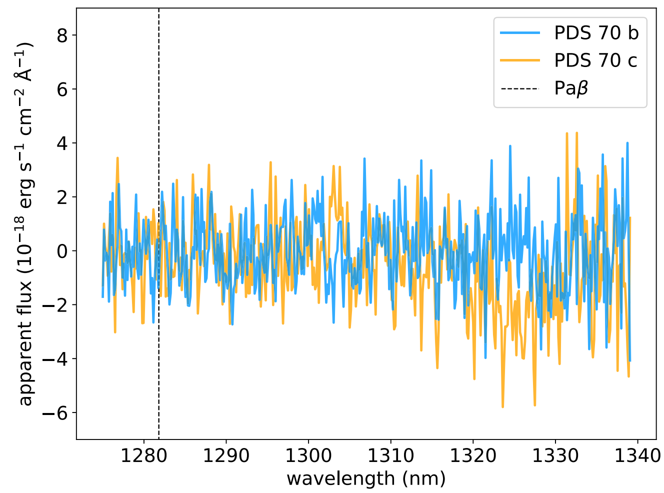

Figure 2. Spectra of the residuals after the HRSDI reduction at the locations of PDS 70 b and c. For display purposes, no throughput correction was made.

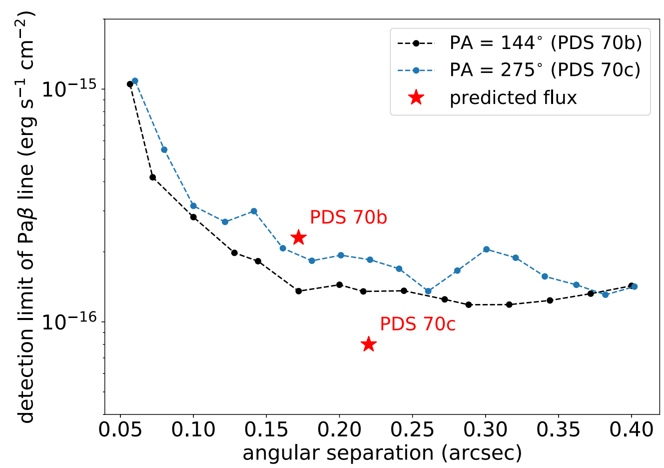

Figure 3. Radial profiles of 5σ detection limits at two position angles. The predicted Paβ fluxes of PDS 70 bc assuming the estimated parameters of Hashimoto et al. (2020) are indicated by the red stars.

3. Results

After the postprocessing as mentioned in Section 2.2 we did not detect Paβ at the locations of PDS 70 b and c (see Figure 1). Figure 2 shows the residual spectra after the HRSDI reduction at the location of PDS 70bc. We then calculated the 5σ detection limits[20] of 1.4×10^{-16} erg s^{-1} cm^{-2} and 1.9×10^{-16} erg s^{-1} cm^{-2} for PDS 70b and c, respectively. The correction of the flux loss caused by the PSF subtraction and the low Strehl ratio has been taken into account. Figure 3 shows the radial profiles for 5σ detection limits at the two position angles of the two planets. We note that the PSF of OSIRIS is not circularly symmetric. Although PDS 70 c is further away from the star, the noise at the location of PDS 70 c is higher, resulting in a higher detection limit.

Uyama et al. (2021) defined the noise as a standard deviation of a spectral channel at the location of PDS 70 b after the SDI reduction without taking into account the OSIRIS' spectral resolution and flux loss by the postprocessing. Their calculations also used the literature value of PDS 70 J-band flux ($J = 9.553$ mag; Skrutskie et al. 2006) to convert the contrast limit into a flux detection limit, but the central star is variable due to its activity and potentially also veiling by the circumstellar disk. In this study we used a field star of HD 144609 ($J = 5.459$ mag; Skrutskie et al. 2006) as a photometric reference and calculated a conversion factor from ADU to the apparent flux.

We also investigated the validity of the estimated limits by injecting fake sources. We used Aoyama & Ikoma (2019) to convert the MUSE-based Hα profiles into the Paβ profiles assuming the derived parameters of PDS 70 bc (the number density: $n_0 = 3.8 \times 10^{12}$ cm^{-3}, the gas velocity: $v_0 = 144$ km s^{-1}, and the extinction: $A_{\mathrm{H}_\alpha} = 2.4$ mag) in Hashimoto et al. (2020). Our prediction for the Paβ flux from PDS 70 b is comparable to the actual OSIRIS detection limit. Since we did not detect Paβ emission our model may have overestimated the Paβ flux. Alternatively, Hashimoto et al. (2020) may have overestimated the 10% and 50% widths of the Hα profiles and thus the parameters of n_0 and/or v_0, possibly because MUSE does not have sufficient spectral resolution ($R \sim 2500$). This latter interpretation can explain the difference between the mass measurements from the IR SED (e.g., Stolker et al. 2020; Wang et al. 2020) and the hydrogen-emission lines (Hashimoto et al. 2020). The mass estimate in Hashimoto et al. (2020) using the Aoyama & Ikoma (2019) model is an upper limit on the dynamical mass of PDS 70 b.

4. Discussion

We use our detection limits of Paβ to further constrain the physical parameters of PDS 70 bc with a theoretical model (Aoyama et al. 2018; Aoyama & Ikoma 2019). For a comparison

[20] The 5σ detection limit is defined as the summation of the flux in the aperture on the residual image and five times of the corresponding noise. As mentioned in Section 2.3, the estimated noise (without throughput correction) at the locations of PDS 70 b and c are 2.5×10^{-18} erg s^{-1} cm^{-2} and 2.7×10^{-18} erg s^{-1} cm^{-2}, respectively. The residual fluxes at the locations of PDS 70 b and c are -2.7×10^{-18} erg s^{-1} cm^{-2} and 2.5×10^{-18} erg s^{-1} cm^{-2}, respectively.

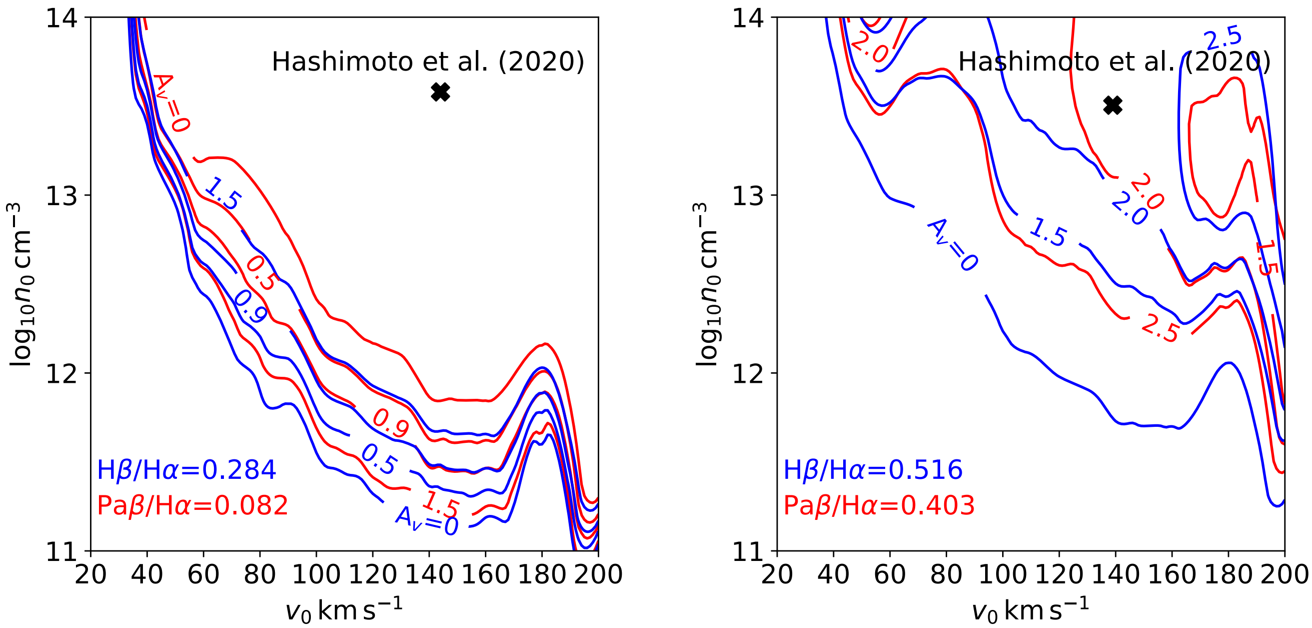

Figure 4. Contours of the 3σ Hβ detection limits (blue; Hashimoto et al. 2020) and the 3σ Paβ detection limits (red; this work) in comparison with the MUSE-based Hα flux of PDS 70 b (left) and PDS 70 c (right). The estimated n_0 and v_0 of PDS 70bc in Hashimoto et al. (2020) are indicated as black crosses respectively. We take into account the extinction effect (A_V) and the wavelength dependency (see Equations (9) and (10) in Wang & Chen 2019). As Hβ is bluer and Paβ is redder than Hα, using these detection limits enables us to set upper and lower limits for A_V, from which we estimate A_V.

with our Paβ detection limits, we refer to: (1) the MUSE results (Hashimoto et al. 2020) which is most similar to the OSIRIS data rather than MagAO or HST because of the similarity of the data format and postprocessing techniques; and (2) the HST results (Zhou et al. 2021) that were obtained in 2020 May close to when we observed PDS 70 with OSIRIS, thereby mitigating any effects of the year-timescale intrinsic variability.

We assume magnetospheric accretion (filling factor of the hydrogen emission—the coverage fraction of the shock on the planetary surface: $f_f \lesssim 0.1$) for the accretion mechanism of PDS 70 bc (e.g., Thanathibodee et al. 2019), from which we can set a lower limit in the (n_0, v_0) parameter space (see also Figure 3 in Hashimoto et al. 2020 for the modeled Hα luminosity with different filling factor values). With this assumption, Hβ and Paβ line strengths are expected to be close to the MUSE and OSIRIS detection limits, respectively. Detailed explanations about the relationship between filling factor, other accretion parameters, and hydrogen-emission luminosity are given in Aoyama et al. (2020). If the filling factor is much larger than the above assumption we cannot simply compare the Paβ limits with the theoretical model. For example, when the shock comes from the circumplanetary disk surface flow rather than the magnetospheric accretion, the filling factor is a few tens of percent (Takasao et al. 2021).

4.1. Comparison between the OSIRIS and MUSE Results

Instrumental differences in the comparison of the visible and IR data should be small since the MUSE and OSIRIS IFSs have similar properties and the two data sets were treated in a similar fashion, using HRSDI to remove the stellar halo and searching for emission lines at small angular separations. We compare our Paβ detection limits with the MUSE-based Hα fluxes. However, we note that we have the uncertainty of time variability due to the difference of the epochs.

We used our 3σ Paβ detection limits (6.6×10^{-17} erg s^{-1} cm^{-2} and 1.3×10^{-16} erg s^{-1} cm^{-2} for PDS 70 b and c, respectively) and the MUSE-based Hα fluxes and 3σ Hβ limits (Hashimoto et al. 2020) to constrain the PDS 70 bc's parameters. Combining the hydrogen-line data from these two AO-fed integral field units provides better constraints on the effects of extinction. The difference of extinction effect between Hβ/Hα and Paβ/Hα ratios enables us to estimate the A_V value. Figure 4 shows the contours of line flux ratio as a function of n_0 and v_0, with a variety of A_V values for PDS 70 b (left) and c (right), respectively. Although our final detection limit is higher than the preliminary result presented in Uyama et al. (2021), the comparison between the Paβ and Hβ limits suggests that A_V for the line emitting region of PDS 70 b is consistent with ∼0.9 ($A_{H\alpha} \sim 0.69$ mag assuming the extinction law in Wang & Chen 2019).

Our extinction estimates are lower than other estimates. Hashimoto et al. (2020) attributed the failure of MUSE to detect Hβ to large extinction ($A_{H\alpha} > 2.0$ mag) but this may be due to the overestimation of (n_0, v_0) and due to the insufficient spectral resolution of MUSE as mentioned in Section 3. Our derived A_V value is also inconsistent with the spectral energy distribution (SED)-fitting argument with the GRAVITY observations ($A_V \sim 4$–10 mag assuming ISM extinction and the best-fit extincted models; Wang et al. 2021) that used the shape of the continuum and the molecular-mapping argument from SINFONI observations ($A_V \sim 16$–17 mag; Cugno et al. 2021), which used the depths of the lines. However, this discrepancy might suggest a vertical difference between the location of the photosphere responsible for the IR-continuum and the hydrogen-emitting regions. The evaporated materials at the shock can sublimate beneath the hydrogen-emitting regions to create an additional extinction source for the PDS 70 b's atmosphere. This assumption does not conflict with the physical assumption of Aoyama et al. (2018). In that sense, IR-continuum observations and hydrogen-emission observations of protoplanets should be careful to identify each extinction effect independently. The large difference between (n_0, v_0) estimated in Hashimoto et al. (2020), and the (n_0, v_0)

contour with $A_V = 0.9$ mag suggests that the filling factor may be larger than a lower limit of Hashimoto et al. (2020) ($f_f \gtrsim 0.01$) by about an order of magnitude. To test the hypothesis about the filling factor, observing the hydrogen-emission line with higher spectral resolution is required. We note that the discussion in this section ignores the time variability as mentioned above. Section 4.2 takes into account the variability effect.

For the case of PDS 70 c, we could not explore as deep parameter space as PDS 70 b because the Paβ detection limit is higher than that of PDS 70 b as mentioned in Section 3 and the Hα flux is smaller (Haffert et al. 2019; Hashimoto et al. 2020). The comparison with the Paβ and Hβ detection limits suggests $A_V \sim 2.0$ mag ($A_{H\alpha} \sim 1.5$ mag). Compared with Hashimoto et al. (2020), who set a lower limit of $A_{H\alpha}$ and f_f to 1.1 mag and $\sim$0.003, respectively, our estimated A_V value is consistent with their argument. We note that this argument relies on the assumption that the Hα profile of PDS 70 c was sufficiently resolved by MUSE. If n_0 and v_0 of PDS 70 c given in Hashimoto et al. (2020) are overestimated as well as those of PDS 70 b, higher contrast levels at Hβ and Paβ are required to constrain these parameters. As mentioned above, PDS 70 c's photospheric continuum may also be extincted by additional material compared with the hydrogen-emitting regions. Resolving the Hα line profile with higher resolution and/or deeper searches for Hβ and Paβ will improve the constraints on the accretion parameters of PDS 70 c.

4.2. Comparison between the OSIRIS and HST Results

As mentioned above, the OSIRIS and MUSE observations were not conducted in the same epoch and thus simply comparing these observational results leaves the uncertainty of the temporal variability. Zhou et al. (2021) monitored PDS 70 b's Hα line with HST between 2020 February and 2020 July, which covers the OSIRIS observation on 2020 May 31 UT, and did not find larger variability in the line flux than 30% ($\sim 2.4\sigma$). They also suggested the hydrogen-line emission was variable on a year timescale by incorporating MagAO and MUSE results obtained in 2018 (Wagner et al. 2018; Hashimoto et al. 2020). In this section we compare our Paβ detection limit of PDS 70 b with the time-averaged Hα flux estimated from the HST observations ($1.62 \pm 0.23 \times 10^{-15}$ erg s^{-1} cm^{-2}; Zhou et al. 2021). Although the HST data format and postprocessing technique are different from OSIRIS, we used injection testing to account for differences in instrumental parameters and data analysis techniques. Figure 5 shows the same contours of PDS 70 b as Figure 4 assuming our Paβ limit and the HST-based Hα flux. Note that we do not include the Hβ limits because the Hβ observations were not conducted at the same epoch. The higher Hα flux value than the MUSE result helps us to explore a deeper parameter space. Assuming that the extinction effect is stable at $A_V = 0.9$ mag, our 3σ detection limit can set an upper limit of v_0 at $\sim$70 km s^{-1}. Using Equation (3) in Hashimoto et al. (2020), this upper limit corresponds to $\sim$3–4 M_{Jup} for the upper limit of PDS 70 b's mass and is consistent with the mass estimation by the IR high-contrast studies (e.g., Stolker et al. 2020; Wang et al. 2020). To better determine/constrain the (variable) accreting parameters simultaneous observations of Hα, Hβ, and Paβ are more helpful.

Zhou et al. (2021) estimated the continuum flux at the wavelength $\lambda = 336$ nm to be $(1.4 \pm 0.3) \times 10^{-18}$ erg s^{-1} cm^{-2} Å^{-1}. This wavelength is located in the hydrogen Balmer continuum. Using the model of Aoyama et al. (2018), we can estimate the fluxes of the hydrogen recombination continua from the shock-heated gas, as a byproduct of the hydrogen-line fluxes. The model prediction can reproduce both the continuum and Hα fluxes observed for PDS 70 b, with some parameter sets. However, our calculation with (v_0, n_0) = (144 km s^{-1}, 3.8×10^{12} cm^{-3}), which is estimated in Hashimoto et al. (2020), resulted in $F_{\lambda,336}/F_{H\alpha} = 5.2 \times 10^{-3}$ Å^{-1}, where $F_{\lambda,336}$ is the flux per unit wavelength at $\lambda = 336$ nm and $F_{H\alpha}$ is the Hα flux, while its observed value is $(8.6 \pm 2.2) \times 10^{-4}$ Å^{-1} when the flux in the F656N filter of HST represents the Hα flux (Zhou et al. 2021). This comparison shows inconsistency with the results of Hashimoto et al. (2020). This implies that the spectral profile given by MUSE can be overestimated, which is consistent with our interpretation about the null detection of Paβ in the OSIRIS observations. Note that the above estimate of (v_0, n_0) comes from the MUSE-based spectral profile. However, the continuum flux for higher values of v_0 is less reliable due to a lack of coolants effective for hot gases in the Aoyama et al. (2018) model. Also, a part of photosphere that is heated by the accretion should emit continuum (e.g., Hartmann et al. 2016). Further theoretical studies on planetary recombination continua are essential.

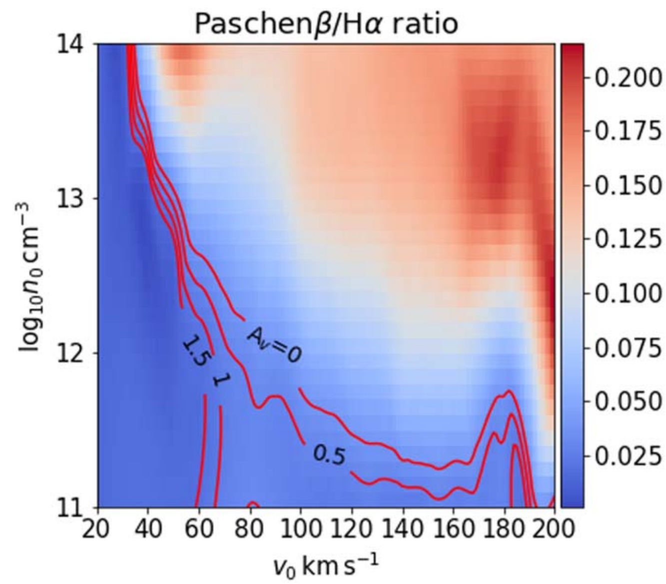

Figure 5. 3σ Paβ detection limit (red) in comparison with the HST-based Hα flux of PDS 70 b. The contours assume $A_V = 0$, 0.5, 1.0, and 1.5 (from top to bottom) and the same wavelength dependency as Figure 4.

5. Summary

We present high-contrast spectral imaging for the unexplored emission line of Paβ from PDS 70 bc with Keck/OSIRIS integral field spectroscopy. After removing stellar halo utilizing the same HRSDI technique that was applied to VLT/MUSE observations, we did not detect Paβ despite the predicted Paβ flux of PDS 70 b from the estimated accretion parameters in Hashimoto et al. (2020) being comparable to the detection limit of our data set. The null detection suggests that our model overestimated the Paβ flux, probably because MUSE does not have sufficient spectral resolution and Hashimoto et al. (2020) overestimated n_0 and v_0 from the Hα profile.

We then compared our detection limits with previous Hα and Hβ observations to set further constraints on the accretion parameters. We adopted two Hα observations from MUSE and HST—comparing OSIRIS with MUSE can assume the smallest systematic difference in terms of the data format and postprocessing techniques, whereas HST covers 2020 May when we observed PDS 70 thereby minimizing the effect of time variability on our conclusions. The MUSE-based comparison between Paβ/Hα and Hβ/Hα ratios enables us to estimate A_V assuming the extinction law. We estimated $A_V \sim 0.9$ and 2.0 for PDS 70 bc, respectively. Particularly the derived A_V of PDS 70 b is inconsistent with the previous NIR studies, but this might suggest an additional extinction source of PDS 70 b's IR-continuum photosphere that is located beneath the hydrogen-emitting regions. The HST-based Paβ/Hα ratio suggested that the year-timescale variation does not significantly affect the A_V estimate. We also incorporated the Balmar continuum detected by HST/WFC F336W observations in the Aoyama et al. (2018) framework. The comparison between the Balmer continuum with Hα flux suggests that the Hα spectral profile may be overestimated. This interpretation is consistent with the null detection of Paβ in our OSIRIS observations.

Higher spectral resolution will resolve the hydrogen-emission line profiles and a deeper search could detect multiple hydrogen emissions, which helps to better estimate the accreting parameters and understand the accretion mechanisms of protoplanets.

We thank Jim Lyke for kindly helping to confirm the OSIRIS FoV settings. The authors would like to thank the anonymous referees for their constructive comments and suggestions to improve the quality of the paper. T.U. is supported by Grant-in-Aid for Japan Society for the Promotion of Science (JSPS) Fellows and JSPS KAKENHI grant No. JP21J01220. Y.H. is supported by the Jet Propulsion Laboratory, California Institute of Technology, under a contract with NASA. K.W. acknowledges support from NASA through the NASA Hubble Fellowship grant HST-HF2-51472.001-A awarded by the Space Telescope Science Institute, which is operated by the Association of Universities for Research in Astronomy, Incorporated, under NASA contract NAS5-26555. The results reported herein benefited from collaborations and/or information exchange within NASA's Nexus for Exoplanet System Science (NExSS) research coordination network sponsored by NASA's Science Mission Directorate.

The data presented herein were obtained at the W. M. Keck Observatory, which is operated as a scientific partnership among the California Institute of Technology, the University of California and the National Aeronautics and Space Administration. The Observatory was made possible by the generous financial support of the W. M. Keck Foundation. This publication makes use of data products from the Two Micron All Sky Survey, which is a joint project of the University of Massachusetts and the Infrared Processing and Analysis Center/California Institute of Technology, funded by the National Aeronautics and Space Administration and the National Science Foundation.

We wish to acknowledge the critical importance of the current and recent Maunakea Observatories daycrew, technicians, telescope operators, computer support, and office staff employees, especially during the challenging times presented by the COVID-19 pandemic. Their expertize, ingenuity, and dedication is indispensable to the continued successful operation of these observatories. The authors wish to recognize and acknowledge the very significant cultural role and reverence that the summit of Maunakea has always had within the indigenous Hawaiian community. We are most fortunate to have the opportunity to conduct observations from this mountain.

ORCID iDs

Taichi Uyama https://orcid.org/0000-0002-6879-3030
Chen Xie https://orcid.org/0000-0002-6318-0104
Yuhiko Aoyama https://orcid.org/0000-0003-0568-9225
Charles A. Beichman https://orcid.org/0000-0002-5627-5471
Jun Hashimoto https://orcid.org/0000-0002-3053-3575
Ruobing Dong https://orcid.org/0000-0001-9290-7846
Yasuhiro Hasegawa https://orcid.org/0000-0002-9017-3663
Masahiro Ikoma https://orcid.org/0000-0002-5658-5971
Dimitri Mawet https://orcid.org/0000-0002-8895-4735
Michael W. McElwain https://orcid.org/0000-0003-0241-8956
Jean-Baptiste Ruffio https://orcid.org/0000-0003-2233-4821
Kevin R. Wagner https://orcid.org/0000-0002-4309-6343
Jason J. Wang https://orcid.org/0000-0003-0774-6502
Yifan Zhou https://orcid.org/0000-0003-2969-6040

References

Amara, A., & Quanz, S. P. 2012, MNRAS, 427, 948
Aoyama, Y., & Ikoma, M. 2019, ApJL, 885, L29
Aoyama, Y., Ikoma, M., & Tanigawa, T. 2018, ApJ, 866, 84
Aoyama, Y., Marleau, G.-D., Mordasini, C., & Ikoma, M. 2020, arXiv:2011.06608
Bonnefoy, M., Currie, T., Marleau, G. D., et al. 2014, A&A, 562, A111
Boss, A. P. 1997, Sci, 276, 1836
Christiaens, V., Cantalloube, F., Casassus, S., et al. 2019, ApJL, 877, L33
Cugno, G., Patapis, P., Stolker, T., et al. 2021, A&A, 653, A12
Haffert, S. Y., Bohn, A. J., de Boer, J., et al. 2019, NatAs, 3, 749
Hartmann, L., Herczeg, G., & Calvet, N. 2016, ARA&A, 54, 135
Hashimoto, J., Aoyama, Y., Konishi, M., et al. 2020, AJ, 159, 222
Houk, N., & Smith-Moore, M. 1988, Michigan Catalogue of Two-dimensional Spectral Types for the HD Stars, Vol. 4 (Ann Arbor, MI: Univ. of Michigan)
Keppler, M., Benisty, M., Müller, A., et al. 2018, A&A, 617, A44
Lockhart, K. E., Do, T., Larkin, J. E., et al. 2019, AJ, 157, 75
Lyke, J., Do, T., Boehle, A., et al. 2017, OSIRIS Toolbox: OH-Suppressing InfraRed Imaging Spectrograph pipeline, Astrophysics Source Code Library, ascl:1710.021
Pollack, J. B., Hubickyj, O., Bodenheimer, P., et al. 1996, Icar, 124, 62
Skrutskie, M. F., Cutri, R. M., Stiening, R., et al. 2006, AJ, 131, 1163
Soummer, R., Pueyo, L., & Larkin, J. 2012, ApJL, 755, L28
Spiegel, D. S., & Burrows, A. 2012, ApJ, 745, 174
Stolker, T., Marleau, G. D., Cugno, G., et al. 2020, A&A, 644, A13
Takasao, S., Aoyama, Y., & Ikoma, M. 2021, arXiv:2106.16113
Thanathibodee, T., Calvet, N., Bae, J., Muzerolle, J., & Hernández, R. F. 2019, ApJ, 885, 94
Uyama, T., Hashimoto, J., Beichman, C. A., et al. 2021, RNAAS, 5, 9
Wagner, K., Follete, K. B., Close, L. M., et al. 2018, ApJL, 863, L8
Wang, J. J., Ginzburg, S., Ren, B., et al. 2020, AJ, 159, 263
Wang, J. J., Vigan, A., Lacour, S., et al. 2021, AJ, 161, 148
Wang, S., & Chen, X. 2019, ApJ, 877, 116
Xie, C., Haffert, S. Y., de Boer, J., et al. 2020, A&A, 644, A149
Zhou, Y., Bowler, B. P., Wagner, K. R., et al. 2021, AJ, 161, 244